Site preference of ternary additions in Ni_3Al

Marcel H. F. Sluiter and Y. Kawazoe
Institute for Materials Research, Tohoku University, Sendai 980-77, Japan
(Received 5 August 1994)

An electronic structure method is developed to examine the site preference of impurities in intermetallic compounds. The current method is based on a perturbation of the coherent potential medium, which represents the configurationally random alloy, within the tight-binding formulation of the linear muffin-tin orbital method. It is applied to predicting the site substitution behavior of a large set of impurities in Ni_3Al (γ'). Impurities in this intermetallic compound may occupy exclusively the Ni or Al sublattices, or may exhibit no particular site preference. Although in a number of cases the experimental observations contradict each other, generally the predicted site preferences agree well with the available experimental data.

I. INTRODUCTION

A number of intermetallic compounds hold the promise of retaining high strength at elevated temperatures. Often, lack of ductility at ambient temperature is the main restriction for practical application. In some compounds, it has been shown that alloying with substitutional elements can significantly enhance those low-temperature mechanical properties.[1–10] The γ' phase in the Ni-Al system is an example of such a compound. This Ni_3Al phase takes the cubic $L1_2$ (Cu_3Au prototype) crystal structure which is based on the fcc lattice. In this structure the cube corners are occupied by the Al species, and the face centers are occupied by the Ni species. A substitutional ternary species may occupy exclusively the cube corner sites, the face centered sites, or appear on both types of sites. Particularly in the case where the ternary addition preferentially substitutes Ni on the face centered sites in Ni_3Al, a significant ductilization has been observed.[2–4] Therefore, it is of interest to predict if a third element added to Ni_3Al exhibits a preference for the face centered or the cube corner sites. As there is a large amount of experimental data available on the site preference of ternary additions, the accuracy of theoretical calculations can be verified.

Already, several approaches have been followed to predict the site preference, with a phenomenological thermodynamic model by Guard and Westbrook,[10] with the Miedema model by Ochiai *et al.*,[11] with the cluster variation method by Tso *et al.*,[12,13] and more recently by Wolverton and deFontaine[14] with an electronic structure method, similar in spirit to the work presented in this paper. Electronic structure methods are particularly applicable to this problem because it has been established long ago that site substitution behavior is determined by electronic rather than size factor considerations.[5,10]

Wolverton *et al.* used the direct configurational averaging method[15] in which effective interactions associated with a small cluster are computed by embedding this cluster within an effective medium. This effective medium is represented by taking the average over a small, randomly selected set of about 10 different atomic configurations, thus the name, direct configurational averaging.

In this study, the embedding medium is determined self-consistently with the coherent potential approximation (CPA). The advantage of this method is that it was shown to be the best single-site representation for the random alloy,[16] and that deviations from randomness can be treated analytically by perturbation theory.[17] Hence, analytic expressions for the effective interactions in terms of the electronic structure properties are obtained. Moreover, in the present contribution many ternary additions are studied that have not to our knowledge been considered before.

The method used here does not rely on any experimental data and is equally applicable to site preference in other intermetallic compounds. The electronic structure of the configurationally disordered alloy on the fcc parent lattice of the ternary alloy is computed with the CPA (Ref. 16) within a tight-binding (TB) description.[18] The tight-binding parameters are derived from linear muffin-tin orbital (LMTO) calculations within the atomic sphere approximation (ASA) according to the formalism by Andersen *et al.*[19] The effects of off-diagonal disorder in the tight-binding Hamiltonian have been treated exactly by means of the method of Blackman *et al.*[20] The effective pair interactions (EPI) between the various atomic species were computed with the generalized perturbation method (GPM).[17] Unlike previous theoretical studies,[11–14,21] here the EPI's beyond the nearest-neighbor shell are taken into account. Pair interactions up to and including the sixth neighbor shell were considered in evaluating the site preference. This made it possible to evaluate the effect of the close proximity of antisite defects on the site preference in Ni_3Al.

This paper is organized as follows: a concise description of the electronic structure formalism is presented, the energetics of site preference in $L1_2$-type intermetallic compounds is discussed within the context of a generalized ternary Ising-like model, a simple site preference parameter is introduced and results for a large number of ternary additions are shown. Finally, a comparison with

experimental data and other theoretical determinations is made.

II. FORMALISM

In the tight-binding approximation, the electronic Hamiltonian is expressed as

$$H = \sum_{i,\lambda} |i\lambda\rangle \epsilon_i^{\lambda} \langle i\lambda| + \sum_{i,j,\lambda,\mu} |i\lambda\rangle \beta_{ij}^{\lambda\mu} \langle j\mu|, \tag{1}$$

where $|i\lambda\rangle$ denotes a state vector associated with site i and orbital λ, ϵ is the site- and orbital-diagonal onsite energy, and β represents the two-center hopping integral. The onsite energies ϵ_i and hopping integrals β_{ij} depend on the occupancy of the sites i and j.

In many tight-binding studies only the diagonal disorder, associated with ϵ_i assuming the values ϵ^A or ϵ^B, is treated properly. Here, the off-diagonal disorder (ODD), associated with the disorder in the hopping parameters, is treated exactly within the single-site CPA framework based on the method by Blackman, Esterling, and Berk[20] (BEB) as formulated by Gonis and Garland.[22,23] Although the description given below is in the form of 2×2 matrices applicable to binary systems, the ternary case is completely similar with corresponding 3×3 matrices. In the BEB treatment the matrix locators g_i, Green's functions G_{ij} and hopping integrals are defined as,

$$\hat{g}_i = \begin{pmatrix} p_i^A g^A & 0 \\ 0 & p_i^B g^B \end{pmatrix}, \tag{2}$$

$$\hat{G}_{ij} = \begin{pmatrix} p_i^A G_{ij} p_j^A & p_i^A G_{ij} p_j^B \\ p_i^B G_{ij} p_j^A & p_i^B G_{ij} p_j^B \end{pmatrix} = \begin{pmatrix} G_{ij}^{AA} & G_{ij}^{AB} \\ G_{ij}^{BA} & G_{ij}^{BB} \end{pmatrix}, \tag{3}$$

$$\hat{\beta}_{ij} = \begin{pmatrix} \beta_{ij}^{AA} & \beta_{ij}^{AB} \\ \beta_{ij}^{BA} & \beta_{ij}^{BB} \end{pmatrix}, \tag{4}$$

where the locator associated with the Q species (A,B,...) is given by $g^Q = (z - \epsilon^Q)^{-1}$, the Green's function $G = (z - H)^{-1}$, and the occupation operator p_i^Q equals unity when site i is occupied by a Q atom, and is zero otherwise. The hat over a function indicates that it is a matrix in terms of the site occupation. Note that the locators $\hat{g}_i$ cannot be inverted. We now define an effective medium with its associated self-energy $\hat{\sigma}$ and coherent locator,

$$\hat{g}^{\mathrm{CPA}} = (\hat{z} - \hat{\sigma})^{-1} = \left[\begin{pmatrix} z & 0 \\ 0 & z \end{pmatrix} - \begin{pmatrix} \sigma^{AA} & \sigma^{AB} \\ \sigma^{BA} & \sigma^{BB} \end{pmatrix} \right]^{-1}, \tag{5}$$

with $\sigma^{AB} = \sigma^{BA}$, such that the single-site occupation averaged onsite Green's function $\langle \hat{G}_{00} \rangle$ is equal to the onsite Green's function of the effective medium $\hat{G}_{00}^{\mathrm{CPA}}$,

$$\langle \hat{G}_{00} \rangle = \hat{G}_{00}^{\mathrm{CPA}}. \tag{6}$$

The CPA onsite Green's function is most easily obtained in reciprocal space

$$\hat{G}_{00}^{\mathrm{CPA}} = N_k^{-1} \sum_{\mathbf{k}} (\hat{z} - \hat{\sigma} - \hat{\beta}_{\mathbf{k}})^{-1}, \tag{7}$$

where $\mathbf{k}$ is a reciprocal space vector in the first Brillouin zone and N_k is the number of reciprocal vectors in the first Brillouin zone. The hopping integrals can be Fourier transformed with

$$\hat{\beta}_{\mathbf{k}} = N^{-1} \sum_{i,j} \hat{\beta}_{ij} e^{i\mathbf{k}\cdot\mathbf{R}_{ij}} \tag{8}$$

where $\mathbf{R}_{ij}$ is the vector connecting sites i and j, and N is the number of sites. The single-site averaged onsite Green's function can be computed with

$$\langle \hat{G}_{00} \rangle = \langle [\hat{1} - \hat{g}_i ((\hat{g}^{\mathrm{CPA}})^{-1} - (\hat{G}_{00}^{\mathrm{CPA}})^{-1})]^{-1} \hat{g}_i \rangle \tag{9}$$

which simplifies to

$$\langle \hat{G}_{00} \rangle = \begin{pmatrix} \frac{c^A}{\sigma^{AA} - \epsilon^A - (G^{\mathrm{CPA},AA})^{-1}} & 0 \\ 0 & \frac{c^B}{\sigma^{BB} - \epsilon^B - (G^{\mathrm{CPA},BB})^{-1}} \end{pmatrix}, \tag{10}$$

where c^Q denotes the concentration of the Q species. The equality of Eqs. (7) and (10) implies that $G^{\mathrm{CPA},AB}$ and $G^{\mathrm{CPA},BA}$ vanish, which reflects the fact that a site cannot be occupied by both an A and a B atom simultaneously. Equation (6) is solved iteratively for the coherent locator with a modified averaged t-matrix approximation (IATA) scheme,[24] where the correction to the coherent locator $\Delta\hat{g}^{\mathrm{CPA}}$ is computed from

$$\Delta\hat{g}^{\mathrm{CPA}} = -\frac{\hat{g}^{\mathrm{CPA}} \langle \hat{t} \rangle \hat{g}^{\mathrm{CPA}}}{\hat{1} + \langle \hat{t} \rangle (\hat{G}^{\mathrm{CPA}} + \hat{g}^{\mathrm{CPA}})}. \tag{11}$$

The site averaged t matrix $\langle \hat{t} \rangle$ is given by

$$\langle \hat{t} \rangle = \sum_Q c^Q \hat{t}^Q, \tag{12}$$

where $\hat{t}^Q$ is computed with

$$\hat{t}^Q = \{ \hat{G}_{ii}^{\mathrm{CPA}} + [\hat{1} - \hat{g}^Q (\hat{g}^{\mathrm{CPA}})^{-1}]^{-1} \hat{g}^Q \}^{-1}. \tag{13}$$

The iterations are carried out over the coherent locator rather than over the coherent potential because the latter becomes singular at concentrations approaching zero or one, which is particularly pertinent here, where the ternary species is present only in low concentrations. For the first iteration we guess the coherent locator according to $\hat{g}^{\mathrm{CPA}} = \sum_Q c^Q \hat{g}^Q$. When the iterations have converged the t matrices take a simple form

$$\hat{t}^A = \begin{pmatrix} [G^{\mathrm{CPA},AA} + g^A(1 - a^{\mathrm{CPA},AA} g^A)^{-1}]^{-1} & 0 \\ 0 & (G^{\mathrm{CPA},BB})^{-1} \end{pmatrix}, \tag{14}$$

or completely general,

$$\hat{t}^Q = \begin{pmatrix} (G^{\mathrm{CPA},AA})^{-1} & 0 & 0 \\ \vdots & \vdots & \vdots \\ 0 & [G^{\mathrm{CPA},QQ} + g^Q(1 - a^{\mathrm{CPA},QQ} g^Q)^{-1}]^{-1} & 0 \\ \vdots & \vdots & \vdots \\ 0 & 0 & (G^{\mathrm{CPA},ZZ})^{-1} \end{pmatrix}, \tag{15}$$

where A, Q, and Z denote various atomic species, and $\hat{a}^{\mathrm{CPA}}$ is the inverse of the coherent locator: $\hat{a}^{\mathrm{CPA}} = (\hat{g}^{\mathrm{CPA}})^{-1}$.

The GPM is applied to the CPA with ODD by using the site occupation matrix formulation of the appropriate Green's functions and t matrices. The energy associated with a pair of atoms of type P and Q is given by

$$W_{ij}^{PQ} = -\frac{\mathrm{Im}}{2\pi} \int_{-\infty}^{E_F} d\epsilon \quad \mathrm{Tr}\mathrm{Tr}_{\lambda,\mu} \hat{G}_{ij,\lambda\mu} \hat{t}_{i,\lambda}^P \hat{G}_{ji,\mu\lambda} \hat{t}_{j,\mu}^Q, \tag{16}$$

where P and Q can be of the same type, and where we have used the property that, on a lattice with cubic symmetry and with angular momentum less than three, the t matrices are diagonal with regard to the angular momentum indices λ and μ. The Fermi energy is denoted by E_F. The first trace (Tr) is with respect to the elements in the site occupation matrix. In the GPM the energy per atom of any configuration $E^{\{p_i\}}$, defined by the set of occupation operators, can be written as a sum of two terms

$$E^{\{p_i\}} = E^{\mathrm{CPA}}(c) + \Delta E_{\mathrm{ord}}^{\{p_i\}}, \tag{17}$$

where E^{CPA} is the energy of the reference (CPA) medium, ΔE_{ord} is the ordering energy, and c is the composition, represented by a vector of concentrations $(c^A, c^B, ..., c^Z)$. The ordering energy represents the energy difference between a particular configuration (say with short- or long-range order) and the random configuration, and can be expressed in terms of the pair energies,

$$\Delta E_{\mathrm{ord}}^{\{p_i\}} = \frac{1}{2} \sum_{P,Q} \sum_{i,j} W_{ij}^{PQ} (p_i^P - c^P)(p_j^Q - c^Q) + \cdots . \tag{18}$$

As we are interested in energies per atom for the infinite crystal, the ordering energy can be written more simply

$$\Delta E_{\mathrm{ord}}^{\{p_i\}} = \frac{1}{2N} \sum_{P,Q} \sum_{i,j} W_{ij}^{PQ} (\langle p_i^P p_j^Q \rangle - c^P c^Q) + \cdots, \tag{19}$$

where $\langle p_i^P p_j^Q \rangle$ indicates the expectation value of an ij pair with configuration PQ. Using the relationships

$$\langle p_i^P p_j^Q \rangle = \langle p_i^Q p_j^P \rangle \tag{20}$$

and

$$\sum_Q \langle p_i^P p_j^Q \rangle = \langle p_i^P \rangle = c^P \tag{21}$$

one can regroup terms,

$$\Delta E_{\mathrm{ord}}^{\{p_i\}} = \frac{1}{2N} {\sum_{P,Q}}' \sum_{i,j} V_{ij}^{PQ} (c^P c^Q - \langle p_i^P p_j^Q \rangle) + \cdots, \tag{22}$$

where the prime in the sum over P, Q indicates that $P > Q$, when the atomic species are ranked in numerical order, and where an EPI between the distinct species P and Q has been defined as

$$V_{ij}^{PQ} = W_{ij}^{PP} - W_{ij}^{PQ} - W_{ij}^{QP} - W_{ij}^{QQ}. \tag{23}$$

The EPI takes a positive (negative) value when unlike (like) neighbors are favored. The special form of the t matrix [Eq. (15)] eliminates many terms in the trace over the site occupation, so that a rather simple expression for the EPI is found,

$$V_{ij}^{PQ} = -\frac{\mathrm{Im}}{2\pi} \int_{-\infty}^{E} d\epsilon \quad \mathrm{Tr} \quad \mathrm{Tr}_{\lambda,\mu} \hat{G}_{ij,\lambda\mu} \hat{G}_{ji,\mu\lambda} (\hat{t}_{i,\lambda}^P - \hat{t}_{i,\lambda}^Q) \times (\hat{t}_{j,\mu}^P - \hat{t}_{j,\mu}^Q). \tag{24}$$

The first trace needs to be carried out over the PP, PQ, QP, and QQ blocks of the site occupation matrix only. In order to analyze which energy range contributes to the EPI, the integration can be carried out up to any given energy E, but, of course, the actual EPI's in the alloy are obtained only if the Fermi level is taken as the upper limit of the integration. Equation (24) illustrates that, within the GPM formalism, the EPI between the P and Q atomic species is influenced by the presence of other atomic species only insofar as such other species affect the effective medium.

In general, the EPI's turn out to be negligible when the sites are more than a few nearest-neighbor distances separated from each other.[25] As a consequence the ordering energy can be expressed in terms of a few (typically 4 or 5) EPI's only.

For configurations where the occupancy of every site is known, as in the case of perfectly ordered stoichiometric compounds, Eq. (22) can be simplified, and the ordering energy per atom is given as

$$\Delta E_{\rm ord}(\{p_n\}) \approx \sum_{P,Q}{}' \sum_s q_s^{PQ} V_s^{PQ}$$

with (25)

$$q_s^{PQ} = \frac{z_s}{2}(c^P c^Q - \langle p_i^P p_j^Q \rangle),$$

where the sum runs over the neighbor shells s and z_s refers to the coordination number associated with the sth neighbor shell. The ordering energy per atom of a binary $L1_2$ ordered phase A_3B or AB_3, for example, is expressed simply as

$$\Delta E_{\rm ord} = \sum_s q_s^{L1_2} V_s^{AB}, \tag{26}$$

where $q_s^{L1_2} = -\frac{3}{8}, \frac{9}{16}, -\frac{3}{4}, \frac{9}{8}, -\frac{3}{4}$.

At zero temperature, the favored atomic configuration is found by minimizing the total energy. In the case of comparing atomic configurations at the same composition and on the same underlying lattice, minimization of the ordering energy suffices, because the energy of the reference medium (CPA) is the same, as is apparent from Eq. (17). Comparing the ordering energy of two different configurations amounts to simply comparing the number of like and unlike pairs in the two configurations. Thus when determining the site preference of a certain atomic species in Ni_3Al the number of pairs must be counted for the case where that species occupies the cube corner Al-type site, and for the case where that species is located on the face centered Ni-type site. The condition that only configurations at exactly the same composition are to be compared means that we must distinguish between Al-poor Ni_3Al, where an Al atom has been removed to make room for the ternary species, and Ni-poor Ni_3Al where a Ni atom made room for the ternary species. In the case of Al-poor $Ni_3Al_{1-x}X_x$ (in the limit of vanishing x), one must, therefore, consider these two configurations: (1) an impurity X can occupy an Al (cube corner) site and (2) an impurity may occupy a Ni (face centered) site and as a consequence force a Ni atom to move to an Al site [see Fig. 1(a) and 1(b)]. Subtracting scenario (2) from (1), the following tally of bonds in the nearest-neighbor shell per impurity atom is obtained: 4 X-Ni and 4 Ni-Al pairs are created and 4 Ni-Ni and 4 X-Al pairs are destroyed. Hence, the energy difference between scenario (1) and (2), from now on called the "site preference energy," is given by $\Delta E_{1-2} = -2V_1^{\rm Al-Ni} - 2V_1^{{\rm Ni}-X} + 2V_1^{{\rm Al}-X}$. If ΔE_{1-2} is negative (positive) X will preferentially occupy the Al (Ni) sites. This reasoning can be extended to more distant neighbor pairs which gives $\Delta E_{1-2} = -2V_1^* + 3V_2^* - 4V_3^* + 6V_4^* - 4V_5^* + \cdots$, or, more general,

$$\Delta E_{1-2} = \sum_s Q_s V_s^*, \tag{27}$$

where the Q_s coefficients are given in Table I, and V_s^* is a combination of EPI's,

$$V_s^* = V_s^{\rm Al-Ni} + V_s^{{\rm Ni}-X} - V_s^{{\rm Al}-X}. \tag{28}$$

So far, the X and Ni antisite defects in scenario (2) have been assumed not to affect each other, that is, their separation has been tacitly assumed to be infinite. When the antisite defects are in close proximity, they affect each others neighbor shells so that the Q_s coefficients are slightly modified. In Table I the Q_s coefficients are given for the cases that the X and Ni antisite defects are at various separations r. Fig. 1(b) displays the case where the antisite defects are at distance $[1, \frac{1}{2}, \frac{1}{2}]$ removed from each other.

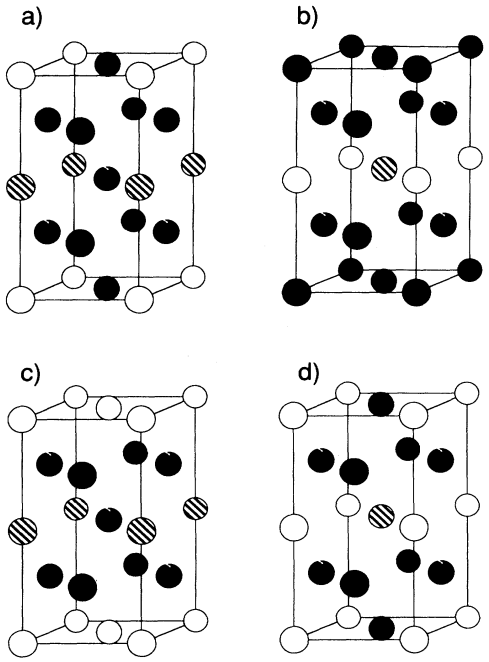

FIG. 1. Atomic configurations that feature the scenarios described in the text: (a) $Ni_6(AlX)$ scenario 1, (b) $(Ni_5X)(AlNi)$ scenario 2, (c) $(Ni_5Al)(AlX)$ scenario 3, and (d) $(Ni_5X)Al_2$ scenario 4.

In the case of Ni-poor $Ni_{3-x}Al_1X_x$ (in the limit of vanishing x), one can derive similar relations. One needs to distinguish between two configurations: (3) an X atom on an Al site with an Al atom on a Ni site, and (4) an X atom on a Ni site with an Al atom in its proper location. The equations are identical except that V_s^* is replaced by V_s^0:

$$\Delta E_{3-4} = \sum_s Q_s V_s^0, \tag{29}$$

where

TABLE I. Q_s coefficients for $L1_2$ structures with antisite defects at various distances from each other.

s	Vector	$r=\infty$	$r=[\frac{1}{2}, \frac{1}{2}, 0]$	$r=[1, \frac{1}{2}, \frac{1}{2}]$	r=$[1\frac{1}{2}, \frac{1}{2}, 0]$
1	$\frac{1}{2}, \frac{1}{2}, 0$	-2	$-1\frac{1}{2}$	-2	-2
2	1, 0, 0	3	3	3	3
3	$1, \frac{1}{2}, \frac{1}{2}$	-4	-4	$-3\frac{1}{2}$	-4
4	1, 1, 0	6	6	6	6
5	$1\frac{1}{2}, \frac{1}{2}, 0$	-4	-4	-4	$-3\frac{1}{2}$
6	1, 1, 1	4	4	4	4

$$V_s^0 = -V_s^{\mathrm{Al-Ni}} + V_s^{\mathrm{Ni}-X} - V_s^{\mathrm{Al}-X}. \quad (30)$$

When ΔE_{1-2} and ΔE_{3-4} are both positive (negative), the impurity X will always occupy the face centered, Ni-type (cube corner, Al-type) sites. When ΔE_{1-2} is negative and ΔE_{3-4} is positive, the impurity will tend towards the Al-type sites in Al-poor, and towards Ni-type sites in Ni-poor alloys. It is important to notice that this concentration dependence of the site substitution behavior does not result from the concentration dependence of the interactions, but instead, is caused by the particular values that these interactions take. The case where ΔE_{1-2} is positive and ΔE_{3-4} is negative is not possible in the zero impurity-concentration limit, as one can see by subtracting ΔE_{3-4} from ΔE_{1-2},

$$\Delta E_{1-2} - \Delta E_{3-4} = \sum_s Q_s V_s^* - Q_s V_s^0 = 2 \sum_s Q_s V_s^{\mathrm{Al-Ni}}. \quad (31)$$

Comparing this difference of site preference energies with the ordering energy of the Ni_3Al $L1_2$ phase [Eq. (26)] gives

$$\Delta E_{1-2} - \Delta E_{3-4} = \frac{32}{3} \Delta E_{\mathrm{ord}}^{L1_2}(\mathrm{Ni_3Al}). \quad (32)$$

The Ni_3Al $L1_2$ phase is stable, and hence its ordering energy is negative. Likewise, the energy difference $\Delta E_{1-2} - \Delta E_{3-4}$ should be negative, which proves that a positive ΔE_{1-2} combined with a negative ΔE_{3-4} is not a realistic scenario. In conjunction with total-energy methods, Eq. (32) can also serve for estimating the ordering energy. By computing the total energies of the structures shown in Fig. 1 one cannot only obtain the site preference, but also, to a good approximation, the ordering energy of the "parent" Ni_3Al phase.

It should be mentioned that the supercells selected here (Fig. 1) allow the prediction of site substitution behavior on both sides of the stoichiometric composition of the intermetallic compound, in contrast to the supercells used in a recent study of the $L1_0$ TiAl compound.[26]

Let us now define a site preference parameter S which takes the values: $S = 1$ when $\Delta E_{1-2} = 0$ (and $\Delta E_{3-4} \neq 0$), and $S = -1$ when $\Delta E_{3-4} = 0$ (and $\Delta E_{1-2} \neq 0$). This assignment is satisfied by the simple expression,

$$S = \frac{\Delta E_{3-4} + \Delta E_{1-2}}{\Delta E_{3-4} - \Delta E_{1-2}}. \quad (33)$$

This definition leads to the following interpretation of the site substitution behavior: $S \geq 1$, X will exclusively occupy the Ni-type sites, $1 > S > 0$, X has a weak preference for the Ni-type sites, $0 > S > -1$, X has a weak preference for the Al-type sites, and $-1 \geq S$, X will exclusively occupy the Al-type sites.

The site preference parameter S can be written in terms of the EPI's using Eqs. (27) and (29),

$$S = \left[\sum_s Q_s (V_s^{\mathrm{Al}-X} - V_s^{\mathrm{Ni}-X}) \right] / \left(\sum_s Q_s V_s^{\mathrm{Ni-Al}} \right). \quad (34)$$

The close proximity of antisite defects is considered by using the appropriate Q factors given in Table I.

III. METHOD

The Slater-Koster parameters used in this study were computed according to the formalism of Andersen *et al.*[19] They have shown that accurate two-center tight-binding parameters can be obtained from LMTO calculations within the ASA. Here, LMTO-ASA calculations were performed for Ni_5Al_2X compounds [Fig. 1(d)] and the resulting potential parameters were used to compute Slater-Koster parameters. Several simplifications were made in the present calculation.

(1) All magnetic moments were ignored, that is, were assumed to be zero. According to full-potential linearized augmented plane wave calculations[27] the energetic difference between ferromagnetic and paramagnetic Ni_3Al is only about 0.1 mRy per atom. This small energy difference is dwarfed by the energies involved in site preferences, which are typically of the same order as the ordering energy. The ordering energy of Ni_3Al is about 7.8 mRy/atom.[28] Moreover, the magnetic moment per Ni_3Al unit cell has an experimental value of only about $0.24\mu_B$.[29] The most accurate theoretical result[27] is about twice as large, $0.46\mu_B$, but is still very small.

(2) Relaxation around the X atomic species was ignored. The computed equilibrium lattice parameter of Ni_3Al was used (0.362 nm) which is about 2% greater than what is observed experimentally (0.356 nm).[30] The c/a ratio of the Ni_5Al_2X structure [Fig. 1(d)] was taken as two. Relaxation around an impurity will lower the total energy. As this will occur regardless of which sublattice the impurity occupies, and as the local environment of both the Al and the Ni sublattices are rather similar (on both sublattices mostly Ni atoms are the nearest neighbors), it is reasonable to expect that relaxation affects the site preference only mildly.

(3) The Slater-Koster parameters were used at compositions that differ from the composition at which those parameters were determined. By extracting Slater-Koster parameters from Ni_6AlX supercells [Fig. 1(a)] for a few selected impurities as well as from Ni_5Al_2X supercells [Fig. 1(d)] it has been verified that this approximation does not change the predicted site preference.

The accuracy of the GPM expansion of the ordering energy can be verified by comparing with supercell calculations. The total energies of the structures depicted in Fig. 1 have been computed with the LMTO-ASA for the case of X=Fe (nonmagnetic). The atomic sphere radii of each atom in the unit cell was taken as the Wigner-Seitz radius and the results are listed in Table II. It must be noted that structures in Figs. 1(b) and 1(c) have antisite defects in close proximity, at a distance $[\ 1, \frac{1}{2}, \frac{1}{2}\ ]$ removed from each other.

In Table III, the site preference energies and site preference as computed from the total energies in Table II and as computed with the GPM using Eqs. (27), (29), and (34) are listed. A comparison of the site preference energies shows that the GPM expansion has introduced

TABLE II. Total energies, in Ry per formula unit, computed with the LMTO-ASA method for the supercells shown in Fig. 1 with X=Fe.

Structure	Total energy
$Ni_6(AlX)$	-21244.602
$(Ni_5X)(AlNi)$	-21244.585
$(Ni_5Al)(AlX)$	-18691.849
$(Ni_5X)Al_2$	-18691.980

an error of about 10 to 20 mRy per Fe atom. However, this error in the energies causes only a very small error in the site preference parameter, a mere 5%. The excellent agreement between the GPM expansion and the total-energy calculations confirms that the CPA-GPM approximations are permissible.

An additional test for the GPM is provided by the ordering energy of Ni_3Al. It can be extracted directly from LMTO-ASA total-energy calculations, and an ordering energy of 14 mRy/atom is found from Eq. (32) and the LMTO-ASA site preference energies in Table III. The GPM result, obtained from Eq. (26) with EPI's from Table IV, is 14 mRy/atom also, in complete agreement with the LMTO-ASA result.

In the GPM, the EPI's are derived from the effective random medium, and hence are composition dependent. In Table IV, the EPI's for Ni-Al-Fe alloys have been computed at various compositions. Clearly, the EPI's vary only weakly in the small region of composition that needs to be considered in this study, and more importantly, no significant change is observed when Ni-poor or Al-poor alloys are considered. Moreover, Table IV illustrates an important feature of the GPM: the EPI's decrease rapidly with increasing distance between the sites. Typically the sixth neighbor, corresponding to a vector [1,1,1], is two orders of magnitude smaller than the first neighbor EPI ($[\frac{1}{2},\frac{1}{2},0]$). The decay of the EPI's with interatomic distance is important because expressions such as (26), (27), (29), and (34) are practical only when the summations can be limited to a few terms.

In LMTO-ASA calculations for alloys, the choice of the atomic sphere radii may affect the results. To verify that our findings are not due to a particular choice of sphere radii, two extreme cases were considered.

(i) Equal sphere radii for the Ni, Al, and X atomic species: this often results in a significant charge transfer. Typically, Ni spheres gain about 0.2 electrons, Al spheres lose approximately 0.3 electrons, and the X spheres tend to lose some charge to Ni as well. Early transition metals (TM) spheres in particular can lose almost one electron to Ni.

TABLE III. Site preference energies, in mRy/Fe atom, and site preference parameter as computed from LMTO-ASA supercell total energies (LMTO), and as computed with the GPM using Q_s coefficients for r=$[1,\frac{1}{2},\frac{1}{2}]$.

Method	ΔE_{1-2}	ΔE_{3-4}	S
LMTO	-17	131	0.89
GPM	-4	145	0.94

TABLE IV. Concentration dependence of the EPI's in $Ni_yAl_{1-y-x}Fe_x$ alloys as computed with the TB-CPA-GPM. The EPI's are given up to the seventh neighbor shell in mRy/atom.

Composition	x	0.02	0.02	0.02	0.05	0.10
	y	0.74	0.75	0.73	0.75	0.75
Type	Shell					
Ni-Al	1	30.7	30.8	30.6	30.5	29.9
	2	-1.5	-1.4	-1.7	-0.9	-0.3
	3	1.6	1.7	1.5	1.8	2.0
	4	-0.2	-0.1	-0.2	-0.1	-0.1
	5	0.0	0.0	-0.0	0.1	0.1
	6	-0.3	-0.3	-0.3	-0.2	-0.1
Ni-Fe	1	-13.3	-13.5	-13.1	-13.1	-12.3
	2	0.2	0.1	0.3	-0.1	-0.3
	3	-1.2	-1.3	-1.1	-1.4	-1.4
	4	0.7	0.7	0.7	0.9	1.1
	5	-0.1	-0.1	-0.0	-0.1	-0.1
	6	0.2	0.1	0.2	0.0	-0.1
Al-Fe	1	18.0	17.2	18.8	15.6	14.2
	2	1.7	1.9	1.5	2.0	1.9
	3	2.2	2.1	2.2	1.7	1.3
	4	-0.7	-0.7	-0.8	-0.7	-0.9
	5	0.1	0.1	0.1	0.1	0.1
	6	0.3	0.4	0.2	0.4	0.3
S		1.07	1.05	1.10	1.00	0.96

(ii) Charge neutral spheres: typically the Al sphere has to be chosen about 10% larger than the Ni sphere. The sizes of the X spheres depend strongly on the position in the Periodic Table, early $4d$ and $5d$ TM's require large radii.

In Fig. 2 the site preference parameters for some elements in the third row of the Periodic Table have been listed as computed with Slater-Koster parameters obtained from LMTO-ASA calculations with equal and charge neutral spheres. For elements to the left (right) of the Ni in the Periodic Table, charge neutrality increases (decreases) the site preference parameter somewhat, but,

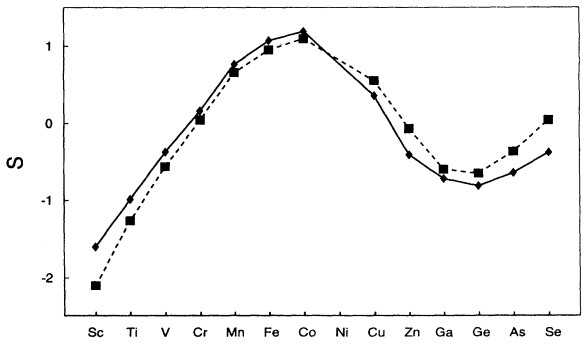

FIG. 2. The predicted site preference parameter S for several elements in the third row of the Periodic Table as computed with Slater-Koster parameters obtained from LMTO-ASA calculations with equal sphere radii (dashed line marked with squares) and with charge neutral spheres (solid line marked with diamonds).

the predicted site substitution behavior itself is not affected. In general, the computed site preference energies are affected quite strongly by the sphere size, typically by as much as 30 mRy/impurity atom, but the predicted site substitution behavior remains unchanged. Only when the site preference parameter is very close to $+1$ or -1, is it possible that the predicted site substitution behavior changes. Such is the case for Fe. Selection of neutral spheres must be considered the more accurate description because it yields more reliable values for the formation energies of compounds,[31] and because it avoids the unphysically large charge transfers that are obtained with equal sphere radii. Of course, the latter argument applies only to ternary elements that have metallic bonding. Equation (32), too, is better satisfied for the charge neutral calculations. From now on all LMTO-ASA calculations shall refer to the case of neutral spheres.

IV. RESULTS

The Ni-Al EPI's (Table IV) are dominated by the very positive first neighbor pair which indicates strong ordering tendencies. When the EPI's are used in conjunction with a ground-state analysis,[32] the $L1_2$ type of ordering is found to be favored, in agreement with experimental observation. The Ni-Al EPI's agree in sign with those computed with the Korringa-Kohn-Rostoker (KKR)-CPA-GPM,[18,28] but differ somewhat in magnitude. In particular, our TB-CPA-GPM gives a larger value for the nearest-neighbor EPI. The ordering energy of Ni_3Al can be computed from the EPI's with Eq. (26), and a value of 14 mRy/atom is found. This is larger than the KKR-CPA-GPM prediction [7.8 mRy/atom (Ref. 28)] and the calorimetric value [7 mRy/atom (Ref. 33)]. Energies that do not depend on the nearest-neighbor EPI, such as the energy difference between $L1_2$ and $D0_{22}$ structures, obtained from our TB-CPA-GPM description agree very well with those obtained from the KKR-CPA-GPM.

In the previous section it was shown that the TB-CPA-GPM reproduced very accurately the site preference energies and the ordering energies. Hence, it appears most likely that the overestimation of the nearest-neighbor EPI is not due to the TB-CPA-GPM approximations. Another LMTO-ASA study[34] too, using a Connolly-Williams type approach, indicates an ordering energy of about 16 mRy/atom. The large difference in the computed ordering energy between LMTO-ASA and the KKR-CPA-GPM is probably due to charge correlations which are ignored in the conventional CPA formalism.[35] It should be emphasized that the ratios of the Ni-X and Al-X EPI's over the Ni-Al EPI, rather than the individual magnitudes of the EPI's determine the site preference, so that relative errors in the individual EPI's tend to cancel out.

In Fig. 3, the nearest-neighbor EPI for several fcc $Ni_{74}Al_{24}X_2$ alloys are displayed. Clearly, the X atomic species do not affect the Ni-Al pair interactions much. This is a direct consequence of the fact that the effective (CPA) medium is not influenced strongly by the presence of 2% X.

The Ni-X and Al-X EPI's are very dependent on the location of element X in the Periodic Table. Ni-X EPI's

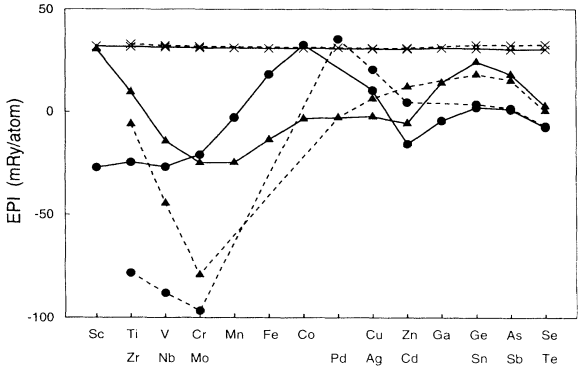

FIG. 3. Nearest-neighbor EPI's in mRy/atom in fcc $Ni_{74}Al_{24}X_2$ alloys for elements X from the third (solid line) and fourth (dashed line) row in the Periodic Table. The Ni-Al, Ni-X, and Al-X EPI's are indicated with crosses, triangles, and circles, respectively.

are repulsive (negative) for early TM's (groups 5B, 6B, 7B), and attractive (positive) for elements in the 3A, 4A, and 5A groups. The attractive EPI's are not surprising considering that Ni forms many stable fcc based ordered intermetallics with 3A, 4A, and 5A elements.

It is not obvious that the EPI's with 5B, 6B, and 7B elements should be negative as Ni also forms many stable intermetallic compounds with these elements. The Al-X interactions are even more repulsive than those for Ni-X for early transition metals. This again, is counterintuitive because the binaries of Al and early TM's exhibit many intermetallic phases. The unexpected sign of the Ni-X and Al-X EPI's is a clear indication that, in general, phase stability trends in binaries cannot be extrapolated far into a ternary system. That the repulsion is most pronounced for the $4d$ and $5d$ early TM's, is probably due to the large size difference.

Late TM's have attractive EPI's with Al which can be explained by a band filling argument.[17,36] Intuitively, attractive EPI's can be expected because elements such as Co and Pd resemble Ni with regard to the scattering properties. This similarity among Co, Pd, and Ni in the electronic properties has several consequences: (1) The scattering between Ni and Co, and Ni and Pd sites is weak and thus the Ni-Co and Ni-Pd EPI's are weak. (2) In the ternary alloy, the interactions between Al and Ni, Co, and Pd remain fairly constant as long as the CPA medium remains the same, that is, at constant Al concentration. It is for this reason that the interactions in the Al-Co and Al-Pd binaries can be extrapolated into the ternary diagram. In the case of an early TM as ternary addition, the CPA medium changes significantly when the TM substitutes for Ni at constant Al concentration, so that one cannot extrapolate EPI's from the early TM-Al binary to the impure Ni_3Al system.

The EPI's between Al and 3A, 4A, and 5A elements are rather weak. Previous work[17,36] has shown that the magnitude of the EPI between two elements P and Q is roughly proportional to the diagonal disorder, that is, the difference in onsite energies of P and Q. The onsite energies of a particular element depend most strongly on the column in the Periodic Table that element is in.

Therefore, especially in the case of Ga and Al, the diagonal disorder is very small, so that weak EPI's between Al and Ga are to be expected. The elements in the 4A and 5A columns too, have only a weak diagonal disorder with Al.

A very appealing feature of the GPM is that the EPI's are expressed in terms of properties of the effective medium, so that there is a direct connection between electronic structure properties and the chemical behavior. In Fig. 4, the electronic density of states (DOS) of two representative $Ni_{74}Al_{24}X_2$ alloys have been displayed. It is clear that the partial DOS of Ni and Al have barely been affected by the third species X, (X=Zr,Se). Correspondingly, the Ni-Al nearest-neighbor EPI for fcc $Ni_{74}Al_{24}X_2$ alloys as computed with Eq. (24) (see Fig. 5) is about the same in the case of X=Zr and X=Se. However, the Ni-X and Al-X EPI's depend strongly on the partial DOS of X.

In the case of Zr two pronounced changes of slope can be discerned in the Ni-X and Al-X EPI curves, at about 0.35 Ry below, and right at the Fermi level. The first change of slope concurs with the sharp peak in the Zr s-like states (see Fig. 6). The second slope change is associated with the rapidly rising p- and d-like Zr states at the Fermi level. The bottom of the band, about 0.9 Ry below the Fermi level, has contributions from all three species and thus the Ni-Al, Ni-Zr, and Al-Zr EPI's all

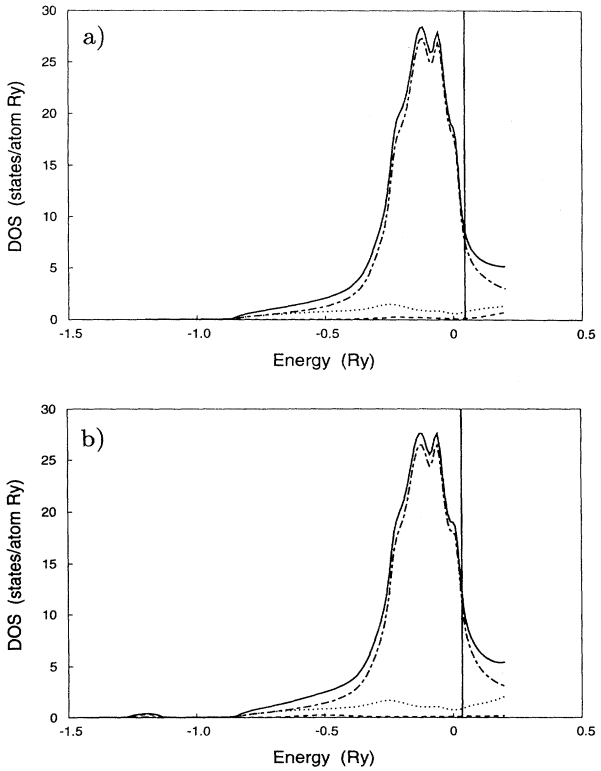

FIG. 4. Electronic density of states (DOS) for fcc $Ni_{74}Al_{24}X_2$ alloys. The vertical line indicates the Fermi level, the solid line represents the total DOS, and the long dash short dash, dotted, and dashed lines indicate the partial DOS of Ni, Al, and X, respectively. (a) X=Zr, (b) X=Se.

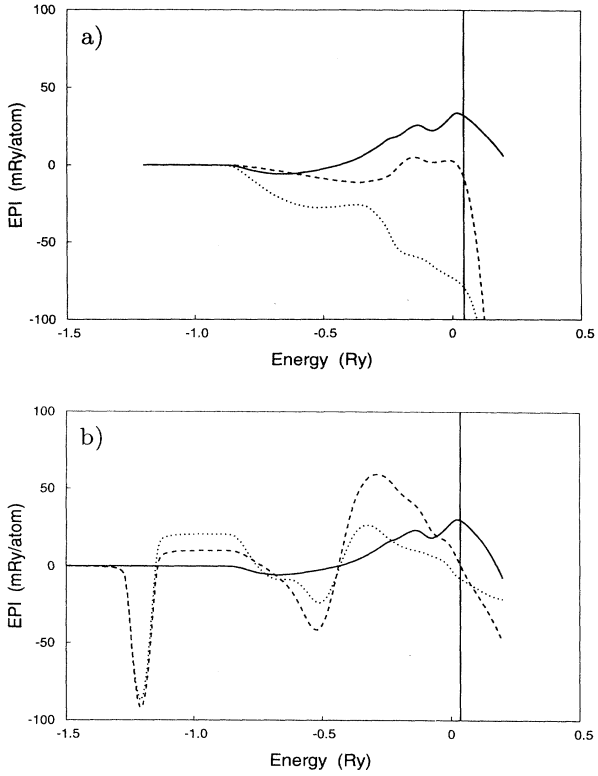

FIG. 5. Nearest-neighbor EPI's in mRy/atom for fcc $Ni_{74}Al_{24}X_2$ alloys as a function of energy. The vertical line indicates the Fermi level, the solid, dashed, and dotted lines indicate the Ni-Al, Ni-X and Al-X EPI's. (a) X=Zr, (b) X=Se.

begin to depart from zero at that energy.

In the case of Se, one notices that the Ni-Se and Al-Se curves differ much from those for Ni-Zr and Al-Zr. The highly localized Se s-states, about 1.25 Ry below the Fermi level, cause a sharp dip in the Ni-Se and Al-Se EPI curves (see Fig. 6). The Se p-like states form a somewhat broader peak in the partial DOS but they too, are clearly reflected in the EPI's. It is possible to precisely pinpoint the electronic origin of the EPI's by a decomposition in terms of angular momentum. A detailed general discussion of the behavior of the EPI's as a function of band filling or, equivalently energy, is found in Ref. 36.

The EPI's have been used to compute the site preference energies [Eqs. (27) and (29)] and the site preference parameter [Eq. (34)] and the results are listed in Table V. In Table VI, the predicted site substitution behavior is compared (a) with deductions from the experimentally determined ternary phase diagrams[37] in the spirit of Ref. 10 and (b) with findings reported in the literature. In previous work[11,14,38] the site preference has been displayed in plots of $V_1^{\mathrm{Al}-X}/V_1^{\mathrm{Ni}-\mathrm{Al}}$ versus $V_1^{\mathrm{Ni}-X}/V_1^{\mathrm{Ni}-\mathrm{Al}}$. We have included such a plot (Fig. 7) to facilitate comparisons.

Table V shows that the difference of ΔE_{1-2} and ΔE_{3-4} is almost independent of the ternary species X, and hence Eq. (32) holds for these alloys with low X concentration.

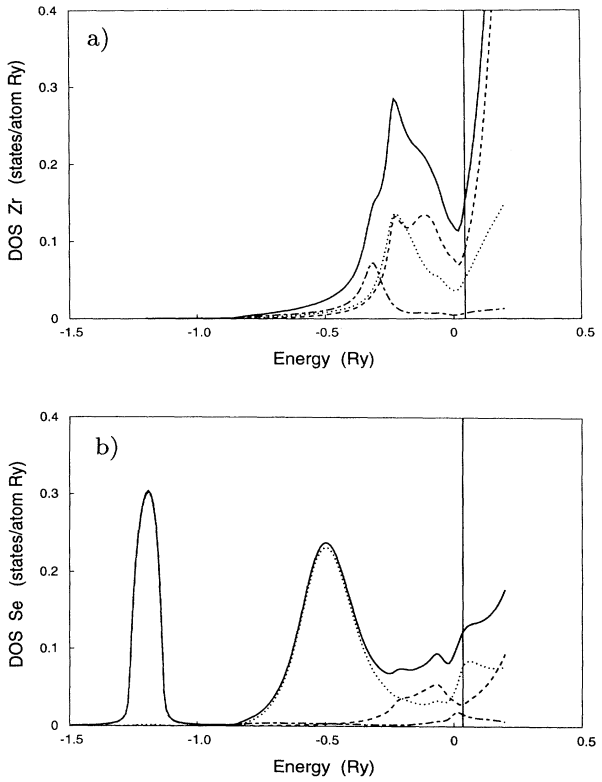

FIG. 6. Partial DOS of X in fcc $Ni_{74}Al_{24}X_2$ alloys. The vertical line indicates the Fermi level, the solid line represents the total X partial DOS, and the long dash short dash, dotted, and dashed lines indicate the s-, p-, and d-like contributions to the X partial DOS, respectively. (a) X=Zr, (b) X=Se.

TABLE V. Predicted site preference behavior of impurities in Ni_3Al. The units for the site preference energies are mRy/impurity atom.

Impurity	ΔE_{1-2}	ΔE_{3-4}	S
Sc	-202	-47	-1.60
Ti	-153	1	-1.00
Zr	-232	-72	-1.91
Hf	-211	-53	-1.66
V	-104	48	-0.37
Nb	-170	-14	-1.18
Ta	-164	-7	-1.09
Cr	-63	88	0.16
Mo	-111	43	-0.45
W	-110	45	-0.42
Mn	-18	133	0.76
Fe	5	155	1.07
Co	14	163	1.19
Pd	16	166	1.21
Cu	-48	101	0.36
Ag	-44	106	0.41
Zn	-104	44	-0.40
Cd	-95	55	-0.27
Ga	-130	21	-0.72
Si	-142	8	-0.89
Ge	-136	14	-0.81
Sn	-123	34	-0.57
As	-120	26	-0.64
Sb	-121	35	-0.55
S	-99	39	-0.43
Se	-99	45	-0.37
Te	-106	50	-0.36

As was seen in Fig. 3, early TM's and Al strongly repel each other. Consequently, scenario 1, in which the impurity occupies an Al-type site and thus avoids Al nearest neighbors, is much favored over scenario 2, in which the impurity occupies a Ni-type site which has four Al nearest neighbors. It is for this reason that early TM's have a strong preference for the Al sublattice. The site preference is especially strong for early TM's in the 4d and 5d series, and rather weak for those in the 3d series.

The direction of the solubility lobe in the experimentally determined ternary phase diagram[10] clearly supports the theoretical result: the solubility lobes extend in the direction of constant Ni concentration for Ti, Hf, V, Nb, Ta, and Mo.[10,11,37,38] Other theoretical work[11,39] also reports a strong Al-site preference for early TM's. In the case of Hf, ion field microscopy[40] and electron channeling[41] agree with our result. Two other investigations with the perturbed angular correlations technique[42] and Rutherford backscattering and ion channeling analysis,[43] however, concluded that Hf should occupy the Ni-type sites. Based on the phase diagram data, the experimental work,[40,41] and the univocal theoretical calculations in this work and elsewhere,[11,39] as well as the strong Al site preference of the other early TM, the authors conclude that the result in Refs. 42 and 43 is not plausible. Clearly, the experimental determination of site preference is not trivial.

The ternary phase diagram of Ni-Al-Sc (Refs. 37 and 44) does not confirm the predicted strong Al-type site preference of Sc. Other theoretical works are contradictory: both Al-site[39] and Ni-site[11] preference are reported. We have found that Cr has no significant site preference, in agreement with the experimentally determined direction of solubility lobe[37,38] and the work by Ochiai *et al.*[11] In contrast, an empirical pair potential model[39] has predicted that Cr should be found on the Ni sublattice.

For Mo and W this work predicts that there is only a weak preference, so weak that in Ni-poor Ni_3Al both Mo and W are expected to occupy the Ni sublattice. This contradicts the experimental ternary phase diagram[37] in the case of Mo, but it is in good agreement with experimental work on extracted precipitates[45] and x-ray diffraction data.[46–48] For Mn a weak preference for the Ni-site is predicted. The Miedema model[11] too, predicts a Ni-site preference. However, ternary phase diagram data give contradictory indications: Refs. 10 and 37 data point to a strong Al sublattice preference, and Refs. 11 and 38 data indicate that no strong site preference should occur. It appears that a weak Al-site preference for Mn is the most likely situation. Our result does not predict this and the authors believe that the neglect of magnetism may be the source of the disparity.[49]

TM's close to Ni in the Periodic Table are predicted to

TABLE VI. Comparison of site preferences as computed in this work and as reported in the literature. An *A* (*N*) indicates that an element will substitute exclusively on the Al (Ni) sublattice both in Al-poor and Ni-poor alloys, or, equivalently, $S < -1$ ($S > 1$); an *a* (*n*) indicates a preference for the Al (Ni) type sites which is too weak to cause antisite defects and hence is composition dependent, and 0 indicates the absence of site preference. Cases where it is known only that the site preference is neither of *A* nor *N* type have been indicated with the letter *c*. "Ternary" refers to deductions made from the direction of the solubility lobe in the ternary phase diagram (see text). "Theory" refers to theoretical determinations reported in the literature, and "experiment" refers to a variety of experimental determinations (see text).

Impurity	This work	Ternary	Theory	Experiment
Sc	*A*	*n* (Refs. 44, 37)	*A* (Refs. 39),*N* (Ref. 11)	
Ti	*A*	*A* (Refs. 10, 11, 37, 38)	*A* (Refs. 39, 11)	*A* (Refs. 58, 45, 46)
Zr	*A*	*A* (Ref. 11)	*A* (Refs. 39, 11)	
Hf	*A*	*A* (Refs. 37, 11)	*A* (Refs. 39, 11)	*A* (Refs. 40, 41),*N* (Refs. 42, 43)
V	*a*	*A* (Refs. 10, 11, 37, 38)	*A* (Refs. 39, 11)	*A* (Refs. 45, 46)
Nb	*A*	*A* (Refs. 11, 37, 38)	*A* (Refs. 39, 11)	*A* (Refs. 45, 46)
Ta	*A*	*A* (Refs. 11, 37, 38)	*A* (Refs. 39, 11)	*A* (Refs. 45, 46),*N* (Ref. 57)
Cr	0	0 (Refs. 10, 37, 38)	*N* (Ref. 39),*A* (Ref. 11)	*c* (Refs. 45, 46)
Mo	*a*	*A* (Refs. 11, 37, 38),*c* (Ref. 10)	*c* (Ref. 39),*A* (Ref. 11)	*c* (Refs. 58, 46–48)
W	*a*	*A* (Refs. 11, 37, 38)	*c* (Ref. 39),*A* (Ref. 11)	*c* (Refs. 58, 46)
Mn	*n*	*A* (Refs. 10, 37),*c* (Refs. 11, 38)	*N* (Ref. 11)	
Fe	*N*	*A*/*N* (Ref. 37),0 (Ref. 10),*N* (Ref. 38)	*N* (Refs. 39, 11)	*a* (Refs. 52, 53), *O* (Ref. 54),*N* (Ref. 45)
Co	*N*	*N* (Refs. 10, 37, 38)	*N* (Refs. 39, 11, 14)	*N* (Refs. 45, 46, 50)
Pd	*N*	*N* (Ref. 37)	*N* (Refs. 11, 14)	*N* (Ref. 51)
Cu	*n*	*N* (Refs. 37, 38)	*N* (Ref. 11),*n* (Ref. 14)	*N* (Ref. 55)
Ag	*n*			
Zn	*a*	*A* (Ref. 37)	*a* (Ref. 14)	
Cd	0			
Ga	*a*	*A* (Ref. 11)		
Si	*a*	*A* (Refs. 10, 11, 37, 38)	*a* (Ref. 14)	
Ge	*a*	*A* (Refs. 11, 37)		*A* (Ref. 56)
Sn	*a*	*A* (Refs. 11, 37)		
As	*a*			
Sb	*a*	*A* (Refs. 11, 37)		
S	*a*			
Se	*a*			
Te	*a*			

favor the Ni sublattice. These late TM's have strongly attractive EPI's with Al and seek to optimize Al nearest neighbors, and hence scenario 4 is favored over scenario 3. In the case of Co and Pd the Ni sublattice preference is well established,[10,11,14,37–39,45,46,50,51] for Fe, however, there are contradictory results. Mössbauer spectroscopy[52] has indicated a rather weak, composition dependent, preference for the Al sublattice. Channeling enhanced microanalysis[53] points to the absence of any significant site preference, as the majority of Fe atoms was found on the Ni sublattice in Ni-poor alloys, and was found on the Al sublattice in Al-poor alloys. A recent *K*-edge extended x-ray absorption fine structure study (Ref. 54) concluded that Fe should have an almost exclusive site preference for the Al sublattice, but, unfortunately, only Al-poor alloys were studied so that it was only proved that Fe cannot have a strong site preference for the Ni sublattice. On the basis of analysis of extracted precipitates Kriege and Baris[45] concluded that Fe should have a preference for the Ni site. However, this conclusion has been questioned.[5]

Analysis of the ternary phase diagram does not lead to a clear conclusion either: The Ni_3Al single phase region reported in Ref. 38 extends along constant Al concentration, indicative of Ni-site substitution behavior, but in Ref. 10 the lobe is aligned between constant Ni and constant Al concentrations, indicative of the absence of site preference. The isothermal sections in Ref. 37 display a rotation of the direction of the solubility lobe as a function of temperature. At high temperatures (950 °C and 1050 °C) it is aligned approximately in the direction of constant Al concentration, indicative of a Ni-site preference, and at lower temperature (750 °C) it is pointed towards constant Ni concentration, indicative of Al-site preference. This rather unusual feature is not found in any other Ni-Al-*X* system. Our calculation, in which magnetism has not been taken into account, clearly disagrees with the low-temperature portion of the phase diagram and the mentioned experimental investigations but it appears to reproduce the high-temperature behavior. In a forthcoming publication[49] the effect of magnetism on the site preference will be explored.

Both Cu and Ag are found to have but a weak preference for the Ni sublattice. In the case of Cu, this finding agrees with another electronic structure study,[14] but there is evidence[37,38,55] that in actuality the Cu-site pref-

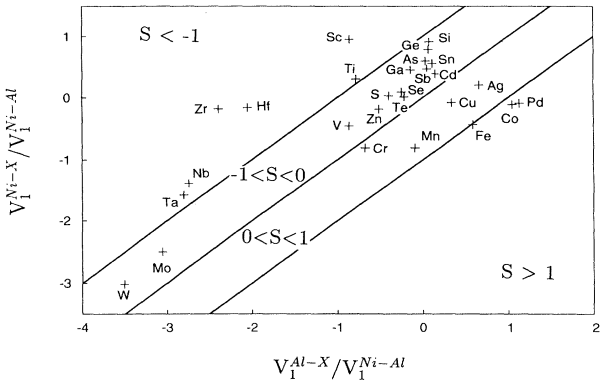

FIG. 7. Predicted site substitution behavior of impurities in Ni_3Al. The region labeled "S< −1" ("S> 1") represents a strong site preference for the Al (Ni) sublattice both in Al-poor and Ni-poor alloys, and the regions labeled "$-1 < S < 0$" ("$0 < S < 1$") represent a weak site preference for the Al (Ni) sublattice, where the site substitution behavior is composition dependent.

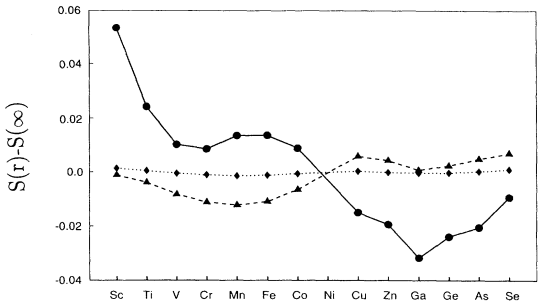

FIG. 8. Effect of proximity of antisite defects on the computed site preference parameter S for several elements in the third row of the Periodic Table. The solid line (circles) represents the change in S resulting from antisite defects being at a distance $r = [\frac{1}{2}, \frac{1}{2}, 0]$ from each other, and the dashed (triangles) and dotted (diamonds) lines indicate the cases where $r = [1, \frac{1}{2}, \frac{1}{2}]$ and $r = [1\frac{1}{2}, \frac{1}{2}, 0]$, respectively.

erence is stronger than predicted.

Zn and Cd have weak preferences for the Al sublattice. In the case of Zn this prediction is also computed by Ref. 14 and can be deduced from the ternary phase diagram[37] as well. The site preference for the Al sublattice is somewhat stronger for Ga, Si, and Ge which is supported by experimental evidence.[11,37,38,56] The remaining 4A, 5A, and 6A elements all have rather weak Al sublattice preferences. For Sn and Sb only, there are ternary phase diagrams available,[37] both of which confirm these predictions.

Aside from visualizing the site preference, Fig. 7 also gives an indication of the solubility of an impurity in Ni_3Al. Impurities that have very repulsive EPI's with both Al and Ni cannot be expected to be very soluble. Indeed, impurities located in the lower left corner, W, Mo, Ta, Nb, and Zr do not have large Ni_3Al single phase fields even in high-temperature isothermal sections of the ternary phase diagrams.[5,10,37] The limited solubility is a consequence of the large size mismatch between the impurity and Ni and Al atoms.

In contrast to earlier studies,[12–14] here pair interactions beyond the nearest-neighbor shell have been included. Therefore, it is possible to take into account the effect of the proximity of antisite defects. In Fig. 8, the change in the site preference parameter $S(r \neq \infty) - S(r = \infty)$ as a function of the distance between antisite defects is shown. The "proximity effect" is shown to be extremely small, in fact much smaller than the accuracy of our computation. Hence, the approximation made in previous work[12–14] is quite adequate. Moreover, we conclude that rather small supercells, such as those shown in Fig. 1, which have rather small distances between the antisite defects, are suitable for the prediction of site preference.

V. CONCLUSION

A method for the prediction of site preference in multicomponent ordered intermetallic compounds has been presented. The method is predictive and does not rely on fitting to experimental data. The application to site preference in Ni_3Al gave results that agree well with available experimental data: Early TM's and Si and Ge were found to substitute preferentially for Al, whereas Fe, Co, and Pd were found to have a strong preference for the Ni sublattice. Cr and Cd were predicted to have virtually no site preference, and elements in the 3A, 5A, and 6A group had but a weak Al sublattice preference. In the case of Cu and Ag a weak Ni sublattice preference was found. Shortcomings of our current predictions are the neglect of magnetism which may affect our predictions for Fe and Mn.[49] It appears that in the case of Cu the site preference is somewhat underestimated. We have also shown that site substitution behavior in Ni_3Al is predominantly driven by the nearest-neighbor EPI so that small supercells can be used in total-energy calculations for the prediction of site preference.

ACKNOWLEDGMENTS

The authors wish to thank Dr. Mark van Schilfgaarde and Dr. Prabhakar P. Singh for making their LMTO-ASA programs available to us. We also are very grateful to Professor S. Hanada, Dr. K. Hono, and Dr. M. Takahashi at IMR, Tohoku University for discussions, to Dr. J.-L. Yu for assistance with computer usage, and to Dr. Chris Wolverton for sharing his results with us prior to publication. One of the authors (M.S.) gratefully acknowledges the visiting professorship provided by Hitachi Corporation and the hospitality of The Institute for Materials Research at Tohoku University.

[1] K. Aoki and O. Izumi, J. Jpn. Inst. Metals **43**, 1190 (1979).
[2] A. Chiba, S. Hanada, and S. Watanabe, Acta Metall. **39**, 1799 (1991).
[3] A. Chiba, S. Hanada, and S. Watanabe, Scr. Metall. Mater. **25**, 303 (1991).
[4] A. Chiba, S. Hanada, and S. Watanabe, Mater. Trans. Jpn.

Inst. Met. **31**, 824 (1990).
[5] R.D. Rawlings and A.E. Staton-Bevan, J. Mater. Sci. **10**, 505 (1975).
[6] S. Ochiai, Y. Mishima, M. Yodogawa, and T. Suzuki, Trans. Jpn. Inst. Met. **27**, 32 (1986).
[7] Y. Mishima, S. Ochiai, M. Yodogawa, and T. Suzuki, Trans. Jpn. Inst. Met. **27**, 41 (1986).
[8] C.T. Liu, C.L. White, and J.A. Horton, Acta Metall. **33**, 213 (1985).
[9] P.H. Thornton, R.G. Davies, and T.L. Johnston, Metall. Trans. **1**, 207 (1970).
[10] R.W. Guard and J.H. Westbrook, Trans. Metall. Soc. AIME **215**, 810 (1959).
[11] S. Ochiai, Y. Oya, and T. Suzuki, Acta Metall. **32**, 289 (1984).
[12] N.C. Tso and J.M. Sanchez, Mater. Sci. Eng. **A108**, 159 (1989).
[13] Y.P. Wu, N.C. Tso, J.M. Sanchez, and J.K. Tien, Acta Metall. **37**, 2835 (1989).
[14] C. Wolverton and D. de Fontaine, Phys. Rev. B **49**, 12 351 (1994).
[15] C. Wolverton, G. Ceder, D. de Fontaine, and H. Dreyssé, Phys. Rev. B **48**, 726 (1993).
[16] J. S. Faulkner, in *Progress in Materials Science*, edited J. W. Christian, P. Haasen, and T. B. Massalski (Pergamon Press, New York, 1982), Vol. **27**, p. 1, and references cited therein.
[17] F. Ducastelle, in *Alloy Phase Stability*, Vol. 163 of NATO Advanced Study Institute Series E: Applied Sciences, edited by G.M. Stocks and A. Gonis (Kluwer, Academic Publishers, Boston, 1989), p. 293, and references cited therein.
[18] M. Sluiter and Prabhakar P. Singh, Phys. Rev. B **49**, 10 918 (1994).
[19] O.K. Andersen, O. Jepsen, and D. Glotzel, in *Highlights of Condensed Matter Theory*, Proceedings of the International School of Physics "Enrico Fermi," Course LXXXIX, Varenna, 1983, edited by F. Bassani, F. Fermi, and M.P. Tosi (North-Holland, Amsterdam, 1985), p. 59.
[20] J.A. Blackman, D.M. Esterling, and N.F. Berk, Phys. Rev. B **4**, 2412 (1971).
[21] M. Kogachi and A. Kameyama, Scr. Metall. **30**, 1089 (1994).
[22] A. Gonis and J.W. Garland, Phys. Rev. B **16**, 1495 (1977).
[23] A. Gonis, *Green Functions for Ordered and Disordered Systems*, Studies in Mathematical Physics Vol. 4 (North-Holland, Amsterdam, 1992), p. 235.
[24] A.-B. Chen, Phys. Rev. B **7**, 2230 (1973).
[25] A. Bieber and F. Gautier, J. Phys. Soc. Jpn. **53**, 2061 (1984).
[26] J.-H. Xu and A.J. Freeman, J. Mater. Res. **9**, 1755 (1994).
[27] J-H Xu, B.I. Min, A.J. Freeman, and T. Oguchi, Phys. Rev. B **41**, 5010 (1990).
[28] M. Sluiter, P.E.A. Turchi, F.J. Pinski, and G.M. Stocks, Mater. Sci. Eng. **A152**, 1 (1992).
[29] F.R. de Boer, C.J. Schinkel, J. Biesterbos, and S. Proost, J. Appl. Phys. **40**, 1049 (1969); N. Buis, Ph.D. thesis, University of Amsterdam, 1979, as quoted in Ref. 27.
[30] *Smithells Metals Reference Handbook*, 6th ed., edited by E.A. Brandes (Butterworths, London, 1983).
[31] M.D. Asta, Ph.D. thesis, University of California, Berkeley, CA, 1993.
[32] J. Kanamori and Y. Kakehashi, J. Phys. (Paris) Colloq. **38**, C7-274 (1977).
[33] S.R. Harris, D.H. Pearson, C.M. Garland, and B. Fultz, J. Mater. Res. **6** (10), 1 (1991).
[34] Z. W. Lu, S. H. Wei, and A. Zunger, Phys. Rev. B **44**, 512 (1991); see Fig. 7(a).
[35] D. D. Johnson and F. J. Pinski, Phys. Rev. B **48**, 11 553 (1993).
[36] M. Sluiter and P.E.A. Turchi, Phys. Rev. **43**, 12 251 (1991).
[37] *Ternary Alloys, a compendium of evaluated constitutional data and phase diagrams*, edited by G. Petzow and G. Effenberg (VCH Publishers, New York, 1993), Vols. 4–8.
[38] C.C. Jia, K. Ishida, and T. Nishizawa, Metall. Trans. **25A**, 473 (1993).
[39] E.S. Machlin and J. Shao, Scr. Metall. **11**, 859 (1977).
[40] M.K. Miller and J.A. Horton, in *High Temperature Ordered Intermetallic Alloys II*, edited by N.S. Stoloff, C.C. Koch, C.T. Liu, and O. Izumi, MRS Symposia Proceedings No. 81 (Materials Research Society, Pittsburgh, PA, 1987), p. 117.
[41] M.K. Miller and J. Bentley, J. Phys. (Paris) Colloq. **47**, **C7**-463 (1986).
[42] H.G. Bohn, R. Schumacher, and R.J. Vianden, in *High Temperature Ordered Intermetallic Alloys II* (Ref. 40), p. 123.
[43] H.G. Bohn, J.M. Williams, J.H. Barrett, and C.T. Liu, in *High Temperature Ordered Intermetallic Alloys II* (Ref. 40), p. 127.
[44] J.A. Goebel and S. Rosen, J. Less-Common. Met. **16**, 441 (1968).
[45] O.H. Kriege and J.M. Baris, J. Less-Common Met. **62**, 195 (1969).
[46] A.V. Karg, D.E. Kornwalt, and O.H. Kriege, J. Inst. Met. **99**, 301 (1971).
[47] E.H. Aigeltinger, S.R. Bates, R.W. Gould, J.J. Hren, and F.N. Hines, in *Proceedings of the International Conference on Rapid Solidification Processing, Principles and Technologies* (Claitor's, Baton Rouge, LA, 1978), p. 291.
[48] W.T. Loomis, J.W. Freeman, and D.L. Sponseller, Metall. Trans. **3**, 989 (1972).
[49] M. Takahashi, M. Sluiter, and Y. Kawazoe (unpublished).
[50] D. Blavette and A. Bostel, Acta Metall. **32**, 811 (1984).
[51] A. Chiba, D. Shindo, and S. Hanada, Acta Metall. **39**, 13 (1991).
[52] J.R. Nicholls and Rees D. Rawlings, Acta Metall. **25**, 187 (1977).
[53] D. Shindo, M. Kikuchi, M. Hirabayashi, S. Hanada, and O. Izumi, Trans. Jpn. Inst. Met. **29**, 956 (1988).
[54] S. Pascarelli, F. Boscherini, S. Mobilio, K. Lawniczak-Jablonska, and R. Kozubski, Phys. Rev. B **49**, 14 984 (1994).
[55] K. Hono, A. Chiba, T. Sakurai, and S. Hanada, Acta Metall. **40**, 419 (1992).
[56] H. Numakura, T. Yamada, M. Koiwa, I.A. Szabo, K. Hono, and T. Sakurai, Defect Diffusion Forum **95-98**, 869 (1993).
[57] H. Lin, L.E. Seiberling, P.E. Lyman, and D.P. Pope, in *High Temperature Ordered Intermetallic Alloys II* (Ref. 40), p. 165.
[58] M.P. Arbuzov and I.A. Zelenkov, Fisika Met. Metalloved. **15**, 725 (1963) [Phys. Met. Metalogr. (USSR) **15**, 71 (1963)]; M. P. Arbuzov, E. T. Kachkovskaya, and B. V. Khayenko, Fizika Met. Metalloved. **21** 854 (1966) [Phys. Met. Metallogr. (USSR) **21**, 46 (1966)], as quoted in Ref. 13.